RSC Advances

ROYAL SOCIETY OF CHEMISTRY

www.rsc.org/advances

Low voltage non-gassing electro-osmotic pump with zeta potential tuned aluminosilicate frits and organic dye electrodes

Harish Lakhotiya, Kunal Mondal, Rajaram K Nagarale, Ashutosh Sharma*
Department of Chemical engineering, Indian Institute of Technology Kanpur, Kanpur-208016, UP, India

Abstract: A novel low-voltage non-gassing electro-osmotic pump using organic-dye electrodes and aluminosilicate frits is demonstrated. Good control of the flow rate is achieved by tuning the zeta potential of the frits in the range of -32.7 mV to -52 mV by varying the aluminum concentration of the aluminosilicate microparticles. The flow rate delivered by the pump is linearly dependent on the zeta potential. The aluminosilicate frits with a maximum zeta potential of -52 mV engendered a maximum flow rate of 27±1.5 μL min^{-1} V^{-1} cm^2. In a continuous operation lasting 11 h, the assembled electro-osmotic pump (EOP) can deliver 7.3 mL of a test solution at 60 μA current density. The flow resulted from concerted shifting of protons generated at the anode by electro-oxidation. The consumption of protons at the cathode was accompanied by decomposition of the dye. The non-gassing pump was operated at 0.5 V, which is well below the thermodynamic potential of water electrolysis. The obtained flow rate and pumped volume is sufficient to deliver a bolus of insulin for diabetes management.

Key words: Electro-osmotic pump, Alizarin, Organic dye, Zeta potential, Silica membrane, drug delivery.

Introduction: Delivering micro-liters of therapeutic drugs at a controlled rate over a long period is often challenging through conventional means. Recently, several technologies and devices have been developed and are being tested to provide precise rates of infusion. Electro-osmotic pumps (EOPs) are arguably the simplest devices that can handle such low volumes. They consist of merely a porous silica membrane sandwiched between two platinum electrodes[1]. EOPs are capable of generating constant, pulse-free flow rate, and pressure. The magnitude and direction of the flow rate can be controlled either by current or voltage. The pumps can be fabricated using standard micro-fabrication technologies and thus can easily be integrated with lab-on-chip devices. Most importantly, they do not have moving parts and hence are more reliable. These types of pumps have been used in various areas, such as chromatographic separations[2-6], lab-on-a chip assays[7-11], microelectronic equipment cooling[12], drug delivery[13, 14], device actuation[15], and fuel cell water management[16].

Conventionally, EOPs are limited to only platinum electrodes and porous silica frits[17-20]. The primary disadvantage of the platinum electrode is the high-voltage operation leading to water electrolysis, generating oxygen at the anode and hydrogen at the cathode. The generated gas bubbles adhere to the electrode and membrane surfaces and block the steady flow of the pump. The first non-gassing EOP was reported in 1977 by Luft, Kuehl, and Richter[21], and it consisted of a polymeric ion-exchange membrane sandwiched between two Ag/AgCl electrodes. The EOP delivered only 0.7 μL min^{-1} at 1 mA cm^{-2}. The very small flow rate of this pump and EOPs developed later[14, 22] failed to satisfy their intended applications. Guzman *et al.* reported rechargeable non-gassing Ag/AgCl electrodes for low-voltage gel electrophoresis of large polyanions in microchannels with 40-100 mM NaCl solutions[22]. Extremely low voltage EOPs have been reported with a 15-nm-thick membrane consisting of porous nanocrystalline silicon, which could provide sufficient flow at voltages as low as 250 mV[23]. Takamura et al.[24] reported an EOP that had a flow velocity of up to 3460 μm s^{-1} at 10 V. Porous alumina membranes containing highly aligned nanochannels modified with silica have shown 86 mL cm^{-2} min^{-1} flow rate[25]. EOPs with track-etched membranes have also been reported[26].

Previously[27-30], we successfully demonstrated a non-gassing, low voltage, and highly efficient electro-osmotic pump based on flows through a consumable Ag/Ag_2O electrode and porous silica frit made of monodisperse silica particles. The protons were generated at the anode by electro-oxidizing Ag to Ag_2O and consumed at the cathode by reducing Ag_2O to Ag. This

highly efficient pump transported 1.3×10^4 water molecules per transported proton. The life of the pump was limited by Ag^+ contamination of the frit, as the adsorbed Ag^+ ions interfered with the transport of protons at the water–membrane interface. To overcome membrane contamination, we are reporting for the first time on an alternative electro material: organic dye alizarin and zeta potential tuned silica frit composed of aluminosilicate micro-particles.

Experimental:

Materials: Tetraethylorthosilicate [TEOS], Aluminum isopropoxide, acetyl acetone, cetyltrimethyl ammonium bromide (CTAB), alizarin, and Nafion solution were obtained from Sigma Aldrich chemicals and used without further purification. Ethanol, isopropanol, and ammonia solution were obtained from Loba chemicals.

Aluminosilicate frits: 8-mm diameter and 1-mm thickness aluminosilicate frits were prepared by fusing 50 mg of aluminosilicate microparticles at 900 ^oC for 4 h. The microparticles were prepared by hydrolysis condensation of TEOS and aluminumisopropoxide in the presence of ammonia and CTAB. In a 100 mL round bottomed flask, solution A was prepared with 10 mL of anhydrous ethanol and equal moles of acetyl acetone and aluminum isopropoxide. TEOS was added to this solution. The molar ratios of TEOS and aluminum isopropoxide were (1:0.1), (1:0.25), (1:0.35), (1:0.5), (1:0.65), and (1:0.75). Solution B was prepared in a 250 mL round bottomed flask by mixing 100 mL ethanol, 59 mL distilled water, 4.847 g CTAB, and 4 mL 25% NH_3 solution under constant stirring. The flask was kept in a water bath at 25 ^oC, and solution A was added. The stirring continued overnight. The white precipitate was filtered, thoroughly washed with ethanol, and dried at 100 ^oC. The surfactant was removed by firing the particles at 500 ^oC for 4 h. Cooled particles were then used to make the frits. All characterizations were performed with particles obtained after grinding the aluminosilicate frit calcinated at 900 ^oC, following which sieving was performed through a mesh of size 320.

Electrodes. The anode and cathode electrode were the same: Alizarin paste coated on a 3.6 cm × 1.8 cm (6.5 cm^2) sheet of 130-μm-thick, 78%-porosity carbon paper (Toray carbon). The carbon paper was treated with a solution of 1% TEOS and 0.1% Triton X-100 before coating. The alizarin paste was prepared by homogeneous mixing of 2 mL 5% Nafion solution, 8-mL isopropanol, 300-mG Alizarin, and 100-mG carbon (TimCal Super-P45). The carbon was made hydrophilic before mixing as follows. To 100-mL distilled water, 1 mL TEOS and 100-mG

Triton X-100 (Sigma-Aldrich) were added. To this well-stirred mixture, 2 g of carbon was added. The stirring was continued for 1 h. The solution was filtered, and the cake was dried at 70 ºC for 6 h. It was then transferred to a silica crucible and fired at 320 ºC for 10 min with 10 ºC/min heating rate. After cooling, it was thoroughly washed with distilled water, dried in an oven at 70 ºC for 6 h and used to produce the paste.

Assembly and pre-conditioning. The pump was assembled in accordance with the procedure given in our earlier report[27]. In brief, an 8-mm diameter electrode–membrane–electrode assembly of volume 0.1 cm^3 and total thickness ~2 mm was sandwiched between two custom-made PVC housings. Silver ring lips were inserted between the electrode and PVC housings as electrical contacts and were encapsulated with fast epoxy resin. After the epoxy dried, the assembly was used for this study.

Electrochemical and flow measurements. Electrochemical measurements were performed using a CHI 760E electrochemical analyzer (Austin, TX). The flow rate was determined by measuring the volume passed through a micro-syringe connected to the outlet of the pump at predefined time intervals.

Instrument details: X-ray diffraction (XRD) measurements were conducted using an X-ray system (X'Pert Pro, PAN Analytical, Netherlands) with Cu Kα radiation (λ = 1.54 Å), to confirm the phase of the synthesized particles. The structures of crystalline materials are typically determined on the basis of Pearson's Crystal Data. The size and morphology of the particles under different synthesis conditions were characterized by field-emission scanning electron microscopy (FE-SEM; Supra 400VP, Zeiss, Germany). The zeta potential of the synthesized aluminosilicate particles calcinated at 900 ^oC in suspension was measured using the dynamic light scattering (DLS) method.

Results and discussion:

The simplest electro-osmotic pumps were assembled as reported[27] with aluminosilicate frits and alizarin as active electrode material. A schematic of the pump, along with the electrode reaction, is presented in Fig. 1. The aluminosilicate frits were prepared from the aluminosilicate microparticles obtained by chemical co-precipitation. SEM micrographs of the microparticles revealed the spherical morphologies shown in Fig. S1 (supporting information). The micro

particles had 200–1000 nm width distribution. Aluminum concentration had a significant effect on the size and shape of the particles. Low concentration favored particles with spherical shape and narrow size distribution (Fig. S1), whereas higher concentration favored particles with irregular shape and size. All the particles were amorphous in nature, which was confirmed through XRD, as shown in Fig. 2. The presence of a broad peak at $2\theta = 22^{o}$ in pure silica confirms the amorphous nature. With the addition of aluminum, an extra peak appears at $2\theta = 27^{o}$, which corresponds to α-alumina, and its peak intensity increases with increasing aluminum content.

Electro-osmotic flow is an electrokinetic phenomenon and results from concerted shifting of protons at the interface between the aluminosilicate surface and water in the frit channels when an electric gradient is applied. At resting, the channels are in equilibrium with negatively charged surface silanol groups (SiOH) and the Stern layer, where protons are tightly held. Positive charges in the Stern layer are usually insufficient to neutralize the negative charges of the surface. Hence, there is a diffuse layer, in which there is a dominance of positive charges. To attain charge neutrality, this diffusion layer, or Debye layer, extends away from the interface into the bulk of the channel. The strong positive charge at the interface is mathematically accounted for by a negative zeta potential (ζ). It serves as a boundary condition for the Debye layer, in which the electrical neutrality between the ions is established only beyond a distance, which is known as the Debye length. When an electric gradient is applied, the concerted shifting of protons at the interface gives momentum to the Debye layer, and hence the resulting bulk water flow. Thus the flow of an electro-osmotic pump is directly proportional to the zeta potential.

To demonstrate experimentally, we successfully tuned the zeta potential of the aluminosilicate frit by varying aluminum concentration, as shown in Fig. 3. With increasing Si/Al mole ratio from 2–10, the magnitude of zeta potential also increased from -32.7 mV to -52 mV. When the Si/Al mole ratio is further increased to 20, the zeta potential magnitude decreased, to -47 mV. This trend suggests that the Si/Al mole ratio defines the number of acidic silanol and aluminol groups existing at the interface. At critical concentration of aluminum; i.e., at 10 Si/Al mole ratio, this results in higher acidic strength to surface –OH functionality. In other words, the bridging hydroxide groups (Si–OH–Al) at the particle surface can be easily de-protonated to form Si–O, making the surface more negatively charged. However, when the Si/Al ratio changes from 10, this effect counteracts the effect of protonation of silanol groups.

The assembled pump was highly efficient and operated at low voltage (0.5 V), which is well below the thermodynamic potential required for electrolysis of water (2.5 V). Because of this low operating voltage, it exhibits a non-gassing operation without the generation of oxygen (anode) and hydrogen (cathode). The assembled pump was approximately 1 mm in diameter and 0.3 cm^2 in cross-sectional active area. Fig. 4 shows the normalized flow rate of the assembled pump, which increases with increasing applied potential. This follows the trend of zeta potential (Table 1). The highest flow rate, 70 ±2 μL min^{-1} cm^{-2}, was obtained at 3 V for -52 mV zeta potential silica frit. We also observed that at higher applied potential, high zeta potential frits provided higher flow. At the lower applied potential; i.e., at 0.5 mV, the zeta potential has no effect on the flow rate, which was 6 ±5 μL min^{-1} cm^{-2} for all frits.

The obtained flow rate, 27±1.5 μL min^{-1} V^{-1} cm^2, with the maximum zeta potential frit is sufficient to infuse a drug, such as a meal-associated bolus of insulin. This flow rate is significantly larger than that previously reported for high-voltage porous glass[31] and ion-exchange membrane EOPs[32], but lower than the 130 μL min^{-1} V^{-1} cm^2 reported for Ag/silica frit/Ag_2O and thin film based EOP[23]. Thin film EOPs assembled with silica coated AAO[25] membranes have reported very high flow rates of 86 mL cm^{-2} min^{-1} at 70 V applied potential. The electro-osmotic pump with the highest reported flow had a 15-nm-thick porous nanocrystaline silicon membrane and Ag/AgCl electrode[23]. It has a normalized flow rate of 260 mL min^{-1} cm^{-2} V^{-1}. The exceptional high flow is described by extremely low transmembrane resistance. Fig. 5A shows the I–V curves for our system. From the slope, we calculated the resistance of the system, which is presented in Fig. 5B. The system has very high resistance, indicating a large portion of the applied voltage drops across the membrane. The actual potential utilized to pump the solution is far less than the applied potential. Compare to our earlier reports[27], the higher pumping resistance of the present pump may be due to the slow redox kinetics, nonconducting nature of alizarin and its insolubility in feed water. In case of Ag/Ag_2O electrodes, it has fast electrode kinetics; good electronic conductor and flushing of silver ion into the feed water decreases the resistivity of the system. This explains the lower flow compared to that of thin-film EOPs.

The main advantage of the alizarin-based EOP is its non-gassing operation and long-term stability. The reported EOPs with Ag/silica frit/Ag_2O[27], which have 2.6 C coulombic capacity

electrodes, can theoretically produce a flow of 6.3 mL of water in 7 h if operated continuously. However, practically, when operated continuously, they have a life span of only 3 h. This short life span is due to fouling of the silica frit by silver ions. However, the EOP assembled with alizarin could operate continuously for 11 h or until the exhaustion of the electrode's coulombic capacity (Fig. 6). This suggests there is no fouling of the silica frit and life of the pump only depends on the electrode's coulombic capacity. The coulombic capacity of the electrodes is 2.4 C, sufficient for 11 h continuous operation at 60 μA, pumping 7.3 mL. But at fixed voltage the flow rate consistently increases with time. The reason may be the continuous change in the equivalent potential of the electrodes and/or change in the membrane properties.

Pump mechanism:

The cyclic voltammograms of an electrode were recorded when cycled between +1.00 and -0.80 V in 10 mM KNO_3 supporting electrolyte. The voltammetric response shown in Fig. 7 indicates two reversible redox waves associated with oxidation reduction of anthraquinone functionalities. The formal reversible potential at about 0.600 mV versus Ag/AgCl is associated with the oxidation reduction of two hydroxyl groups, while the formal reversible potential at about -0.580 mV versus Ag/AgCl is associated with the reduction/oxidation of quinolic groups. This formal potential indicates that it has a half-cell potential of ~1.180 V when a completely oxidized anode and reduced cathode are present. It is the thermodynamic potential required to pump the water under completely oxidized and reduced condition of electrodes. But the resting potential of the alizarin electrode is -0.200 mV versus Ag/AgCl and approximately -0.05 V versus a hydrogen electrode. When both the anode and cathode are identical, the cell potential will be zero. The potential required to pump the solution will be the potential difference of the oxidation and reduction peaks. This is approximately 0.120 V for both the hydroxyl and quinolic functionality of alizarin. This 0.120 V potential is the minimum potential required to operate the pump. The minimum operational potential of the pump is 0.5 V, which is higher than 0.120 V. The higher required potential may be due to the resistivity component of the system.

Fig. 8 shows a schematic of the anodic and cathodic reactions of the electrodes which are responsible for the clean generation and consumption of protons in the present EOP. At the anode, the oxidation of alizarin gives two protons, two electrons, and a tetraquinone alizarin derivative, which is stable and stays on the electrode because of its highly hydrophobic nature. At the cathode, alizarin decomposes into phthalic acid and small organic molecules by

consumption of protons in presence of electrons and oxygen. The mechanism might be similar to the two electron oxygen reduction at antraquinone. The stability of completely reduced alizarin; i.e., the tetrahydroxy derivative, is poor and it continuously decomposes into small molecules[33-35]. The decomposition is associated with the attachment of a cationic radical at the C9 position by active oxygen radicals and/or oxygen. These radicals get scavenged by oxygen which might form the superoxide ion radical $O_2^{\bullet-}$, which further converts to $HOO^{\bullet}$, H_2O_2, and $^{\bullet}OH$ species via a series of protonation, disproportionation, and reduction steps. The C9 atom of the cationic radical is attacked by, and/or combines with, the active oxygen radicals and/or O_2 to result in the formation of an organoperoxide intermediate, which is very unstable. The decomposition of this organoperoxide intermediate leads to the destruction of the conjugated system of the alizarin. The alizarin molecule is cleaved into two parts by O_2 and/or active oxygen radicals; one part is oxidized to phthalic acid, which no longer degrades, has good solubility in water, and comes with pumped water; another part is oxidized to hydroxyl intermediates and finally mineralized to CO_2 and small organic species via a series of complicated oxidation reactions of transient intermediates aldehyde and/or carboxylic acid, similar to the degradation of alizarin dyes as reported elsewhere[36-38].

The generation of phthalic acid at the cathode was confirmed by recording the UV spectrum of the pumped fluid. Fig. 9 shows the UV spectra of the neat alizarin, and pumped water along with 0.5-mM phthalic acid solution. Neat alizarin is sparingly soluble in water. The spectrum was recorded with a solution of alizarin in water, which was prepared by boiling 100 mg of alizarin in 50 mL of distilled water and then cooling and filtering the solution. The spectrum of the filtered solution is shown in Fig. 9(A), and it has the characteristic absorption of alizarin at 260 nm. The spectrum of the pumped water is shown in Fig. 9 (B), and it has a strong absorption at 230 nm. This is the characteristic absorption of phthalic acid in solution, and it was confirmed by recording the UV spectrum of 0.5-mM phthalic acid in water, which has the same absorption as that of the pumped water. This indicates that the decomposition of alizarin occurs at the cathode during the operation of the pump.

Surface morphology of the electrode and membranes before and after operation of the pump is shown in Fig. 10. Before use, the electrode surface had dense, pointed, rod-like crystals of alizarin composite. After use, the morphology changed to porous rod-like crystallite without pointed ends specifically at the cathode. The anode was dense but lost its pointed ends. The

membrane was clean after and before use, no substantial change in surface morphology was observed, and no substantial deposit was observed on the membrane, indicating the absence of membrane fouling by electrode reactions, and hence indicating clean and simple anodic oxidation/reduction of hydroxyl groups of the alizarin to generate protons. This clearly supports the proposed anodic reaction.

Conclusions:

We successfully assembled a low voltage, non-gassing electro-osmotic pump with aluminosilicate frits having different zeta potential and organic dye electrodes. The flow rate was linearly dependent on the zeta potential of the frits. When operated continuously, it could pump water for 11 h or until the electro-active material was exhausted, without fouling of the aluminosilicate frits. The pump delivered 7.3 mL of solution at 60 μA current density in 11 h. Its flow rate showed linear dependence on the applied potential, with a flow rate of 27±1.5 μL min^{-1} V^{-1} cm^2 for the highest zeta potential aluminosilicate frit. This flow rate is sufficient to deliver drugs, such as boli of insulin for diabetes management. It could also be used in a number of other drug infusion systems, in which personal care by health staff is expensive or unreliable. The mechanism of the pump involves the clean electro-oxidation of alizarin dye at the anode and decomposition at the cathode in the presence of H^+, electron, and oxygen.

Acknowledgments: RKN Thanks the Department of Science & Technology (DST), Government of India, for Ramanujan Fellowship (SR/S2/RJN-18/2011) award and financial support, (grant Number SR/S3/CE/034/2013). RKN thanks Prof. Adam Heller, Department of Chemical Engineering, University of Texas at Austin, for his continuous support and fruitful discussion. The encouragement and kind support of Prof. P. K. Bhattacharya, Department of Chemical Engineering, IIT-Kanpur is earnestly acknowledged by RKN.

References

1. X. Wang, C. Cheng, S. Wang and S. Liu, *Microfluidics and Nanofluidics*, 2009, **6**, 145-162.
2. Z. Zhu, H. Chen, W. Wang, A. Morgan, C. Gu, C. He, J. J. Lu and S. Liu, *Angewandte Chemie International Edition*, **52**, 5612-5616.
3. T. D. Mai and P. C. Hauser, *Journal of Chromatography A*, **1267**, 266-272.
4. V. Pretorius, B. J. Hopkins and J. D. Schieke, *Journal of Chromatography A*, 1974, **99**, 23-30.
5. L. Chen, J. Ma and Y. Guan, *Journal of Chromatography A*, 2004, **1028**, 219-226.
6. L. Chen, J. Ma and Y. Guan, *Microchemical Journal*, 2003, **75**, 15-21.
7. J. r. P. Kutter, S. C. Jacobson and J. M. Ramsey, *Analytical Chemistry*, 1997, **69**, 5165-5171.
8. C.-C. Huang, M. Z. Bazant and T. Thorsen, *Lab on a Chip*, 2010, **10**, 80-85.
9. A. G. Hadd, D. E. Raymond, J. W. Halliwell, S. C. Jacobson and J. M. Ramsey, *Analytical Chemistry*, 1997, **69**, 3407-3412.
10. P. C. H. Li and D. J. Harrison, *Analytical Chemistry*, 1997, **69**, 1564-1568.
11. H. Salimi-Moosavi, T. Tang and D. J. Harrison, *Journal of the American Chemical Society*, 1997, **119**, 8716-8717.
12. Y. Berrouche, Y. Avenas, C. Schaeffer, H.-C. Chang and W. Ping, *Industry Applications, IEEE Transactions on*, 2009, **45**, 2073-2079.
13. M. J. Pikal, *Advanced Drug Delivery Reviews*, 2001, **46**, 281-305.
14. L. Chen, J. Choo and B. Yan, *Expert Opinion on Drug Delivery*, 2007, **4**, 119-129.
15. P. Prakash, M. D. Grissom, C. D. Rahn and A. L. Zydney, *Journal of Membrane Science*, 2006, **286**, 153-160.
16. K. Kwon and D. Kim, *Journal of Power Sources*, 2013, **221**, 172-176.
17. D. Kim, J. D. Posner and J. G. Santiago, *Sensors and Actuators A: Physical*, 2008, **141**, 201-212.
18. F.-Q. Nie, M. Macka, L. Barron, D. Connolly, N. Kent and B. Paull, *Analyst*, 2007, **132**, 417-424.
19. S. Yao, D. E. Hertzog, S. Zeng, J. C. Mikkelsen Jr and J. G. Santiago, *Journal of Colloid and Interface Science*, 2003, **268**, 143-153.
20. P. D. Christensen, S. W. P. Johnson, T. McCreedy, V. Skelton and N. G. Wilson, *Analytical Communications*, 1998, **35**, 341-343.
21. G. Luft, D. Kuhl and G. J. Richter, *Biomed. Tech.*, 1977, **22**, 169-173.
22. K. A. D. Guzman, R. N. Karnik, J. S. Newman and A. Majumdar, *J. Microelectromech. Syst.*, 2006, **15**, 237-245.
23. J. L. Snyder, J. Getpreecharsawas, D. Z. Fang, T. R. Gaborski, C. C. Striemer, P. M. Fauchet, D. A. Borkholder and J. L. McGrath, *Proc. Natl. Acad. Sci. U. S. A.*, 2013, **110**, 18425-18430.
24. Y. Takamura, H. Onoda, H. Inokuchi, S. Adachi, A. Oki and Y. Horiike, *ELECTROPHORESIS*, 2003, **24**, 185-192.
25. J. Y. Miao, Z. L. Xu, X. Y. Zhang, N. Wang, Z. Y. Yang and P. Sheng, *Advanced Materials*, 2007, **19**, 4234-4237.
26. C. Wang, L. Wang, X. Zhu, Y. Wang and J. Xue, *Lab on a Chip*, 2012, **12**, 1710-1716.
27. W. Shin, J. M. Lee, R. K. Nagarale, S. J. Shin and A. Heller, *Journal of the American Chemical Society*, 2011, **133**, 2374-2377.
28. W. Shin, S. Shin, J. Lee, R. Nagarale and A. Heller, *Drug Delivery and Translational Research*, 2011, **1**, 342-347.
29. W. Shin, E. Zhu, R. K. Nagarale, C. H. Kim, J. M. Lee, S. J. Shin and A. Heller, *Analytical Chemistry*, 2011, **83**, 5023-5025.
30. R. K. Nagarale, A. Heller and W. Shin, *Journal of The Electrochemical Society*, 2012, **159**, P14-P17.

31. S. Zeng, C.-H. Chen, J. C. Mikkelsen Jr and J. G. Santiago, *Sensors and Actuators B: Chemical*, 2001, **79**, 107-114.
32. A. Brask, J. P. Kutter and H. Bruus, *Lab on a Chip*, 2005, **5**, 730-738.
33. G. Liu, T. Wu, J. Zhao, H. Hidaka and N. Serpone, *Environmental Science & Technology*, 1999, **33**, 2081-2087.
34. G. Liu, X. Li, J. Zhao, S. Horikoshi and H. Hidaka, *Journal of Molecular Catalysis A: Chemical*, 2000, **153**, 221-229.
35. M. Panizza and G. Cerisola, *Water Research*, 2009, **43**, 339-344.
36. A. M. Faouzi, B. Nasr and G. Abdellatif, *Dyes and Pigments*, 2007, **73**, 86-89.
37. A. DomÃ©nech-CarbÃ³ and M. a. T. DomÃ©nech-CarbÃ³, *Electrochemistry Communications*, 2008, **10**, 1238-1241.
38. Y. Di Iorio, H. n. B. Rodrìl guez, E. San Romaì n and M. a. A. Grela, *The Journal of Physical Chemistry C*, 2010, **114**, 11515-11521.

Figure captions

Fig. 1 Schematic presentation of the electro osmotic pump assembly.

Fig. 2 XRD of the aluminosilicate particles recorded at room temperature. The particles were obtained after grinding the frits calcinated at 900 ^{o}C for 4 h. Before recording, the particles were sieved through 320 mesh.

Fig. 3 Dependence of zeta potential of the particles on mole ratio of TEOS to aluminum propoxide. The particles were obtained after grinding the frits calcinated at 900 ^{o}C for 4 h. Before recording the particles were sieved through 320 mesh. The zeta potential was recorded with the dynamic light scattering method in water suspension. *represents the zeta potential of pure silica prepared in the present experiments.

Fig. 4 Dependence of flow rate on the applied potential. The flow rate was measured as reported in[29].

Table 1. Dependence of flow rate on the zeta potential of the particles with varying composition at different voltages.

Fig. 5 Resistance of the aluminosilicate frits calculated from the I-V curves. Inset: I-V curves (♦ = SiO_2), (■ = Si/Al-2), (×= Si/Al-4), (▲ = SiAl-10), (* = Si/Al-20). The reference electrode was platinum.

Fig. 6. Flow rate versus time for the assembled pump operated continuously at 1 V constant applied potential. The pump could perform for 660 min or until the electro-active dye, alizarin, was consumed.

Fig. 7. Cyclic voltammograms recorded in 10 mM KNO_3 electrolyte, with 5 µL of alizarin paste coated glassy carbon as the working substance; Ag/AgCl as reference; and Pt wire as counter electrodes, in air. The scan rate was 10 mV/S.

Fig. 8 Anodic and cathodic reactions of the EOP.

Fig. 9 UV/-visible spectra of alizarin, phthalic acid, and pumped water. The absorption of pumped water at 230 nm confirms the presence of phthalic acid and supports the contention of the decomposition of alizarin.

Fig. 10 SEM images of the electrodes after and before use.

Fig. S1 SEM images of sub-micrometric silica particles doped with different concentrations of alumina. From left to right, particles are at 500 ^{0}C to 900 ^{0}C; top to bottom shows different concentration of alumina in silica particles, by row from the top (silica:alumina): (1:0.1), (1:0.25), (1:0.35), (1:0.5), (1:0.65), and (1:0.75).

Figures

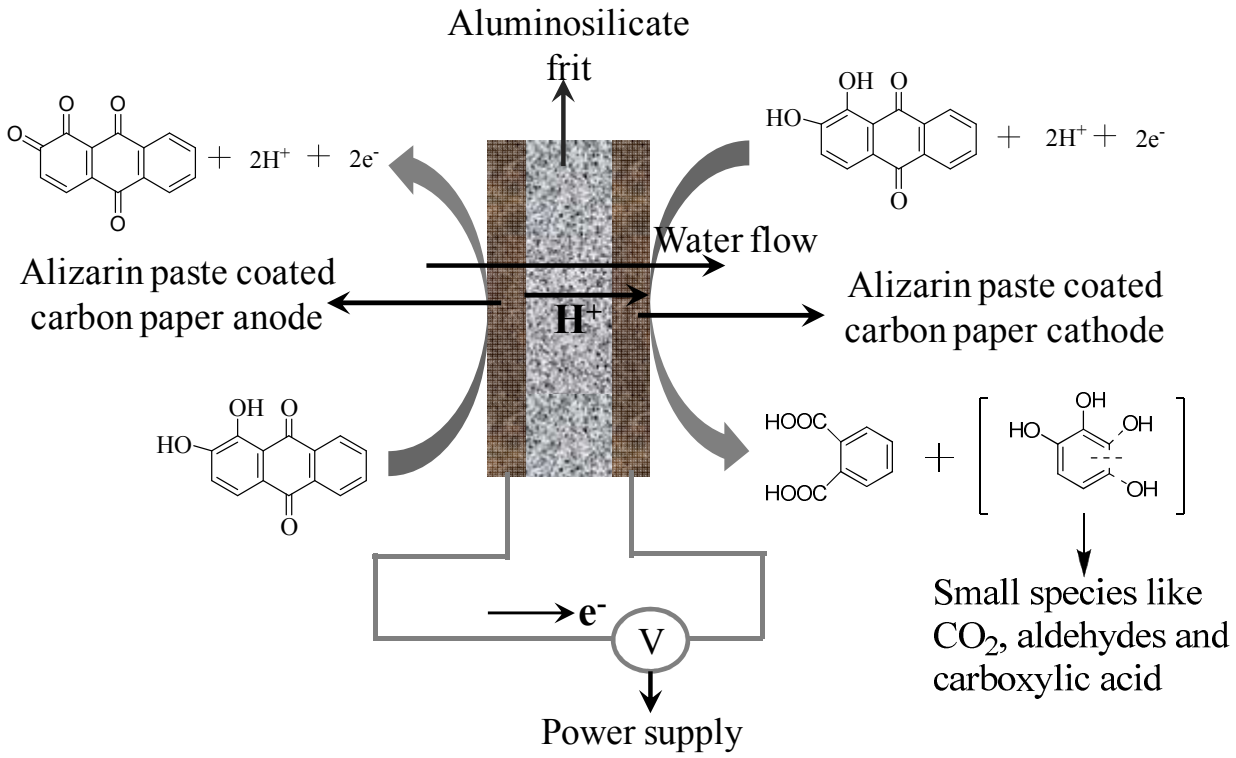

Fig. 1 Schematic presentation of the electro osmotic pump assembly.

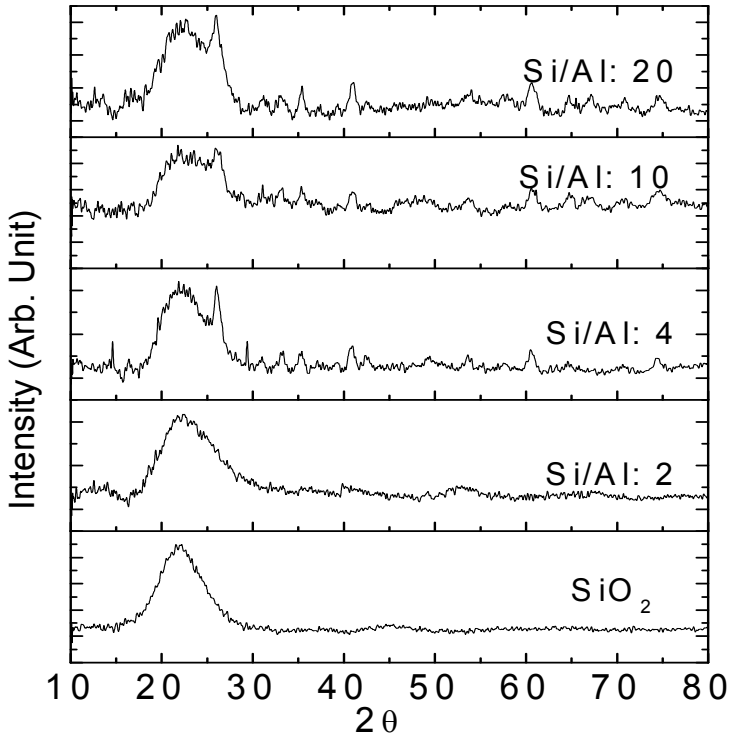

Fig. 2 XRD of the aluminosilicate particles recorded at room temperature. The particles were obtained after grinding the frits calcinated at 900 ^{o}C for 4 h. Before recording, the particles were sieved through 320 mesh.

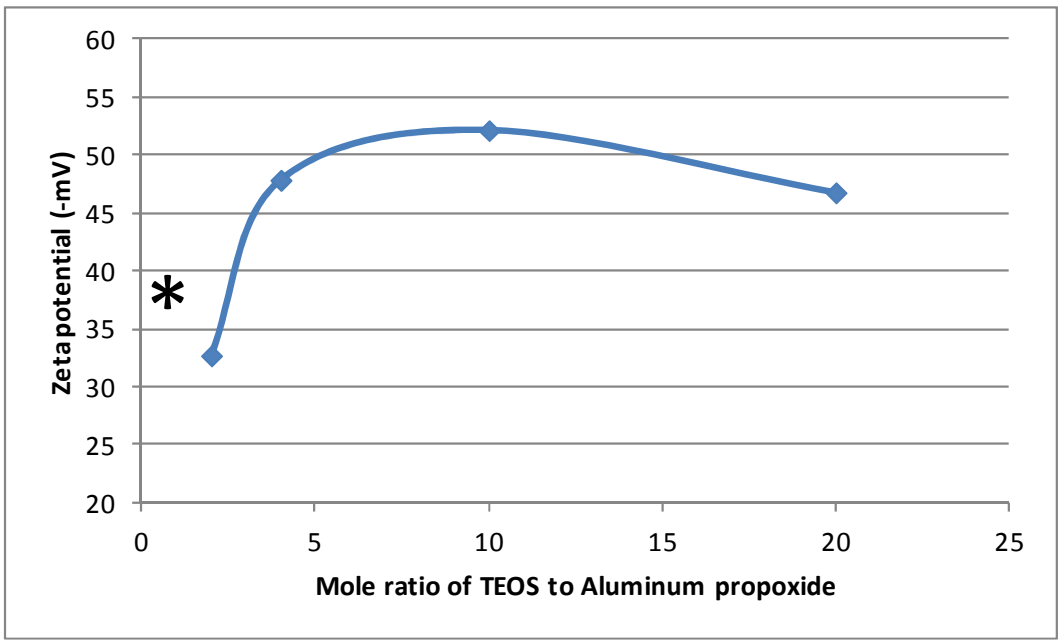

Fig. 3 Dependence of zeta potential of the particles on mole ratio of TEOS to aluminum propoxide. The particles were obtained after grinding the frits calcinated at 900 ^{o}C for 4 h. Before recording the particles were sieved through 320 mesh. The zeta potential was recorded with the dynamic light scattering method in water suspension. *represents the zeta potential of pure silica prepared in the present experiments.

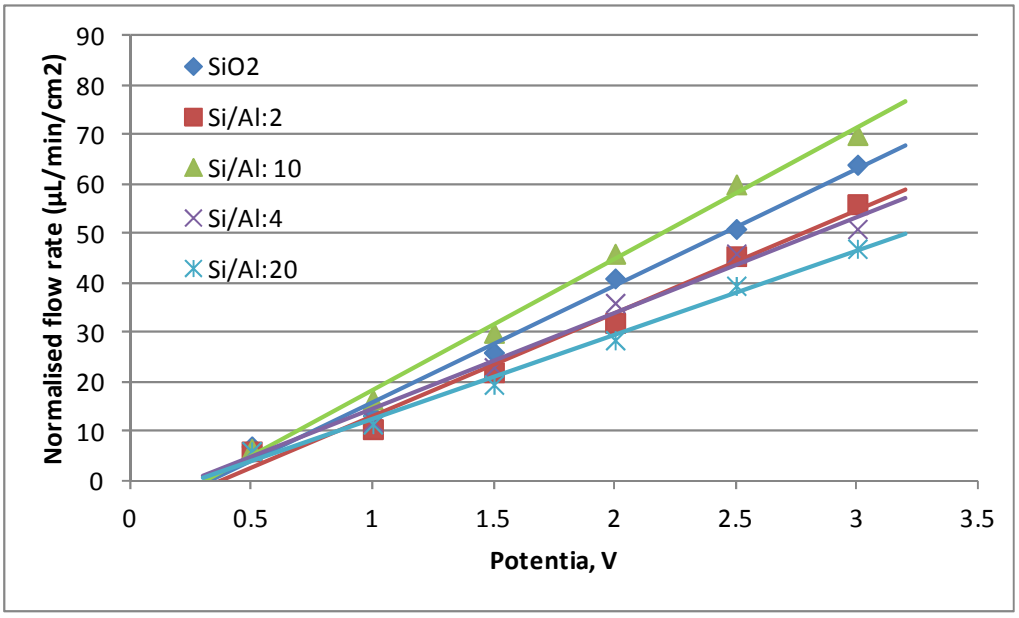

Fig. 4 Dependence of flow rate on the applied potential. The flow rate was measured as reported in[29].

Table 1. Dependence of flow rate on the zeta potential of the particles with varying composition at different voltages

Particle compositions	Zeta Potential	Normalized flow rate (μL/min/cm^2) at different Voltage					
		0.5	1	1.5	2	2.5	3
SiO2	-37.92	7	13.25	26	41	51	64
1:0.05	-46.75	6	10.5	22	32	45.5	56
1:0.1	-52.12	6.5	16.5	30	46	60	70
1:0.25	-47.83	6	12.5	23	36	46	51
1:0.5	-32.69	6	11.5	19.5	28.5	39.5	47

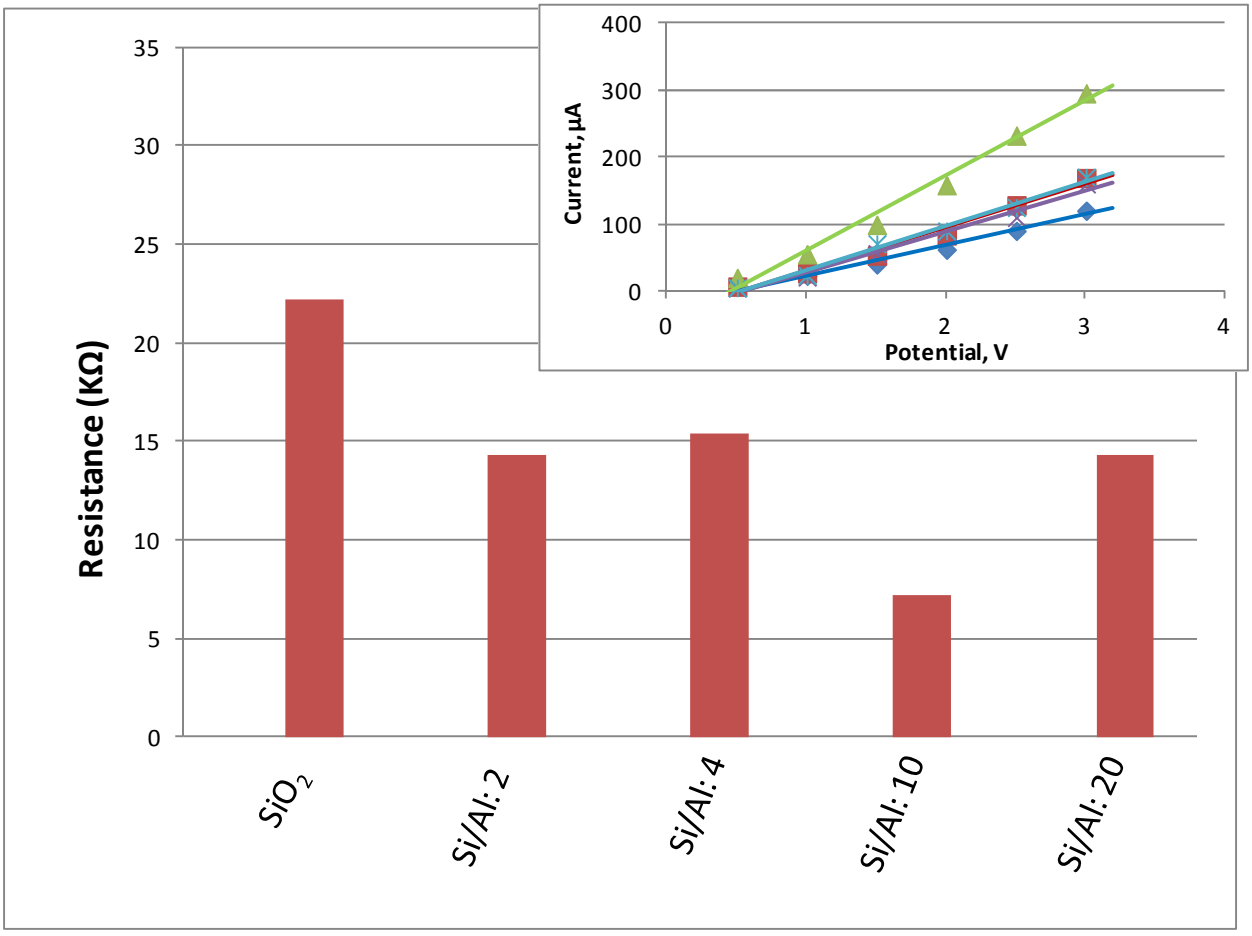

Fig. 5 Resistance of the aluminosilicate frits calculated from the I-V curves. Inset: I-V curves (♦ = SiO_2), (■ = Si/Al-2), (×= Si/Al-4), (▲ = SiAl-10), (* = Si/Al-20). The reference electrode was platinum.

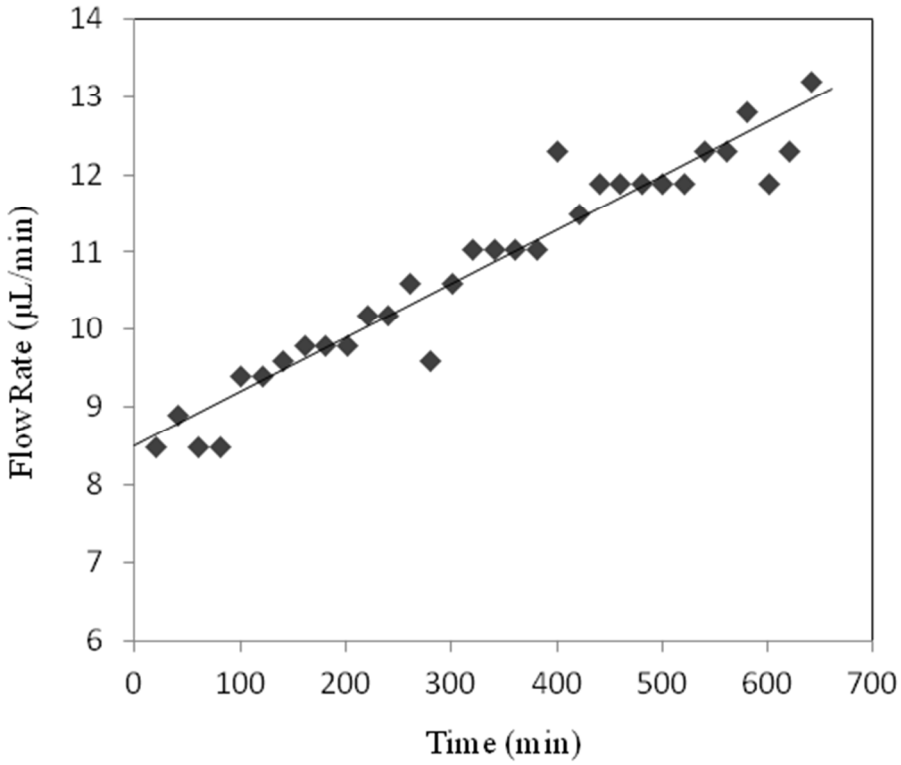

Fig. 6. Flow rate versus time for the assembled pump operated continuously at 1 V constant applied potential. The pump could perform for 660 min or until the electro-active dye, alizarin, was consumed

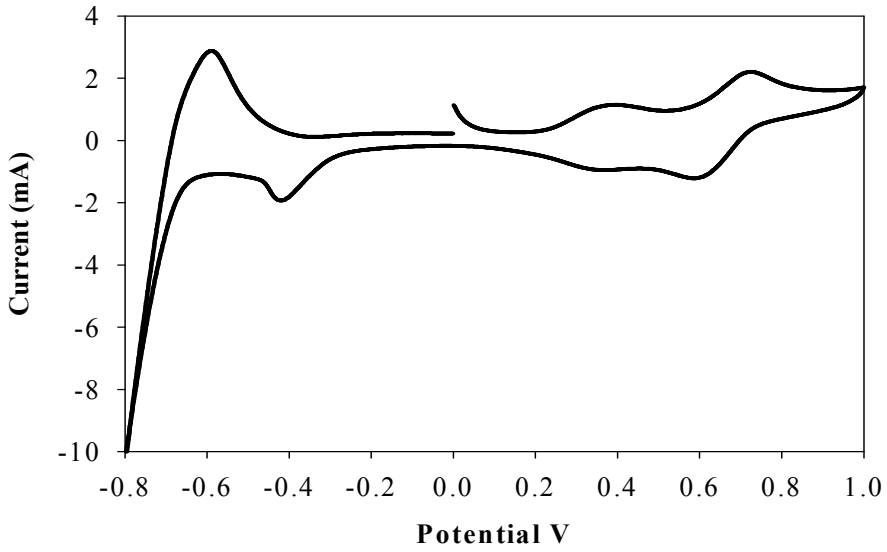

Fig. 7 Cyclic voltammograms recorded in 10 mM KNO_3 electrolyte, with 5 µL of alizarin paste coated glassy carbon as the working substance; Ag/AgCl as reference; and Pt wire as counter electrodes, in air. The scan rate was 10 mV/S.

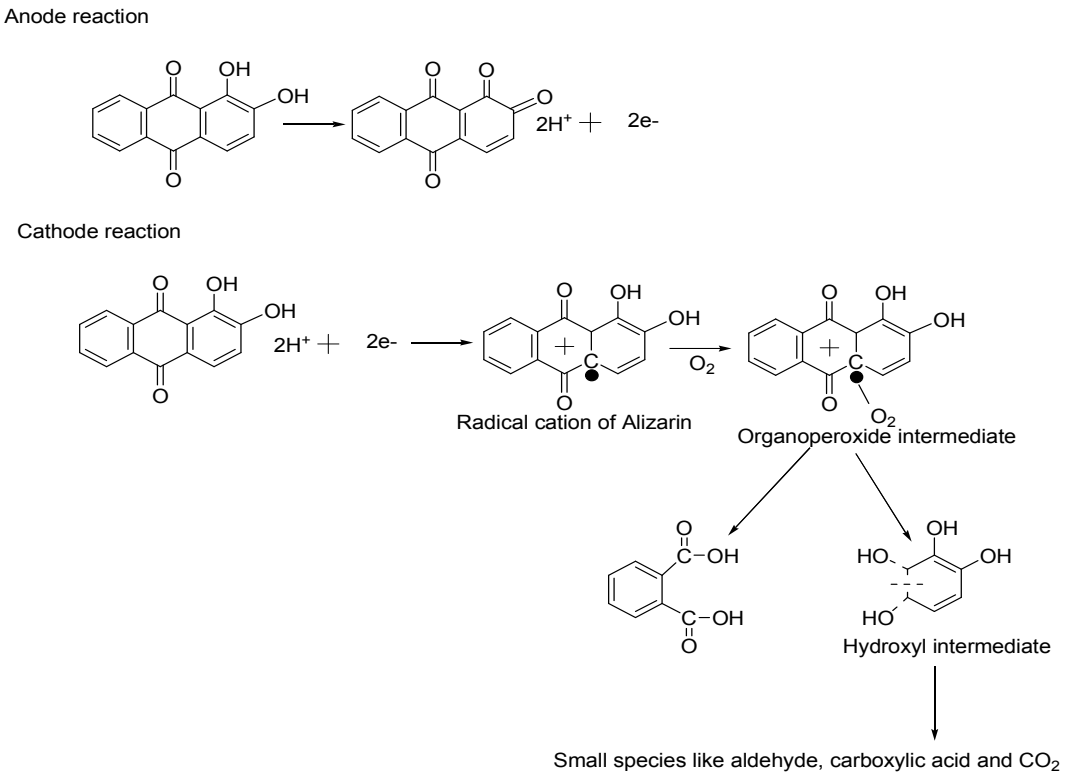

Fig. 8 Anodic and cathodic reactions of the EOP.

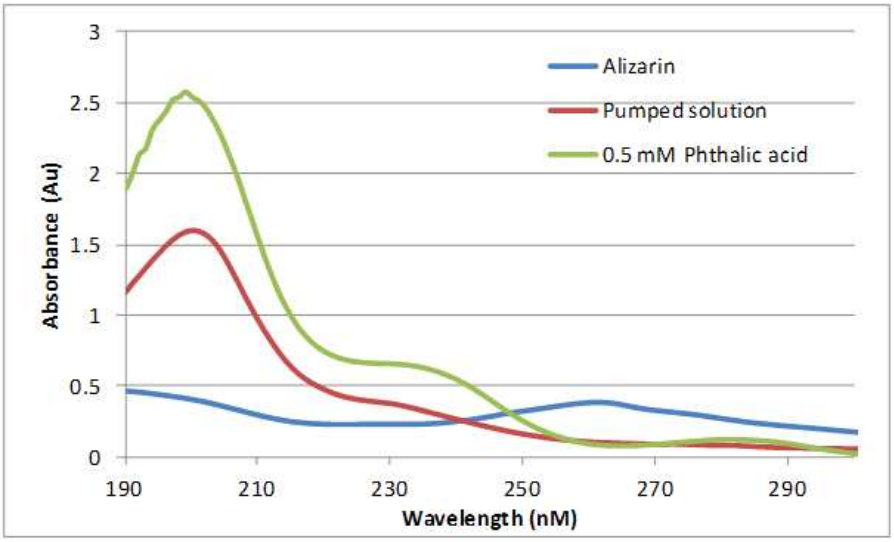

Fig. 9 UV/-visible spectra of alizarin, phthalic acid, and pumped water. The absorption of pumped water at 230 nm confirms the presence of phthalic acid and supports the contention of the decomposition of alizarin.

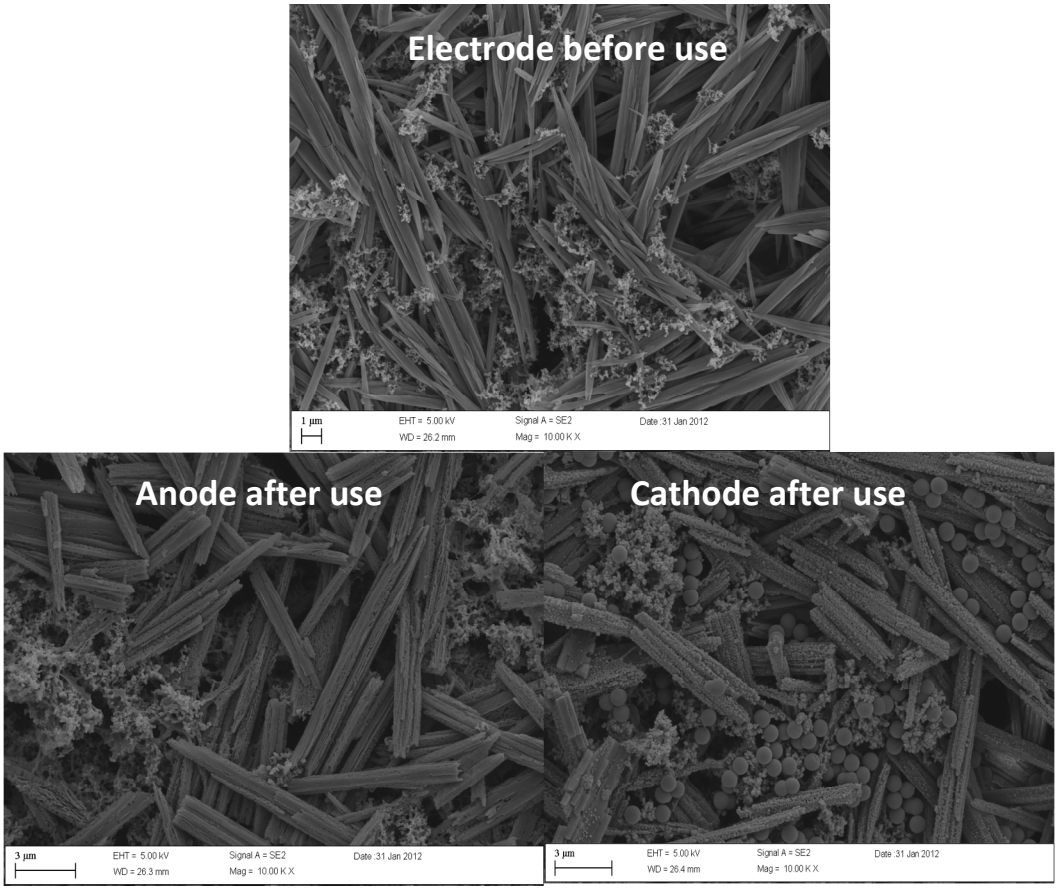

Fig. 10 SEM images of the electrodes after and before use.

Supporting information

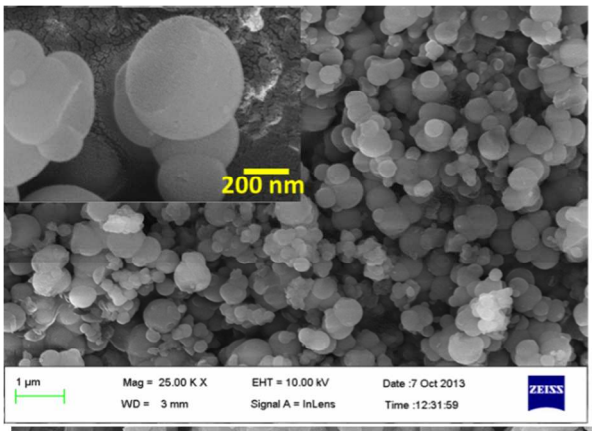

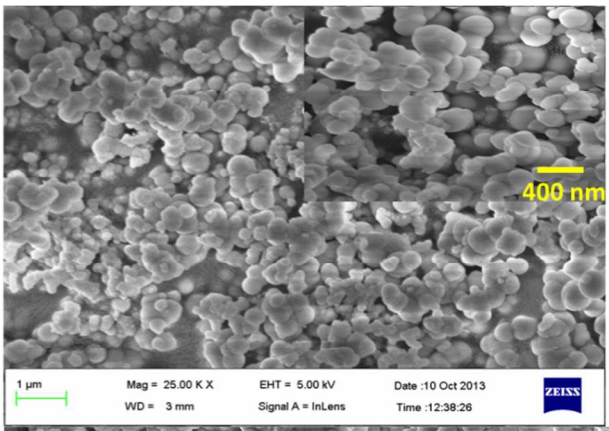

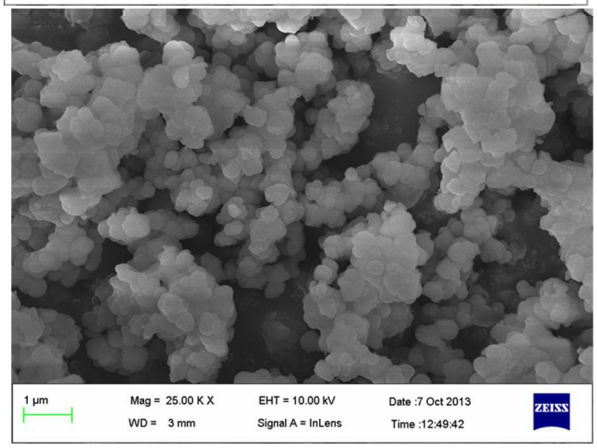

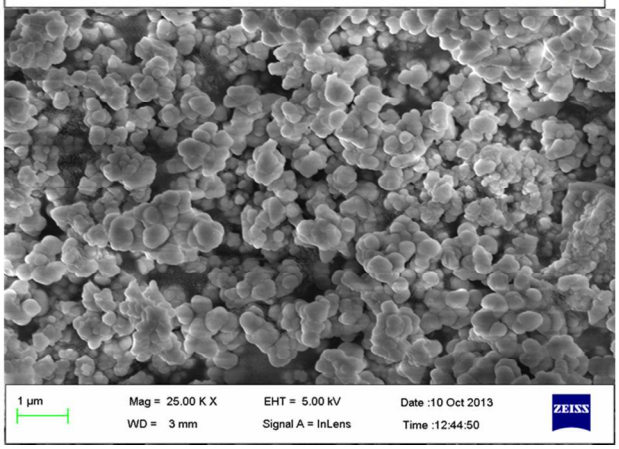

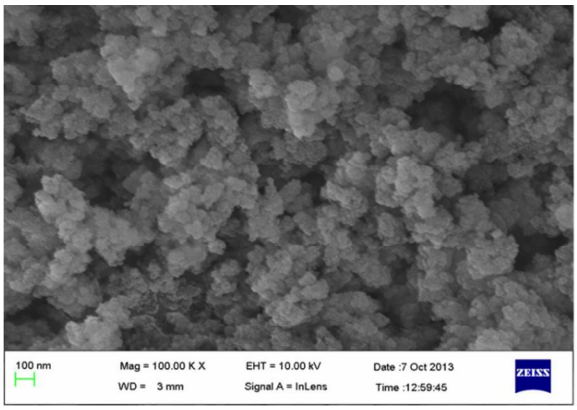

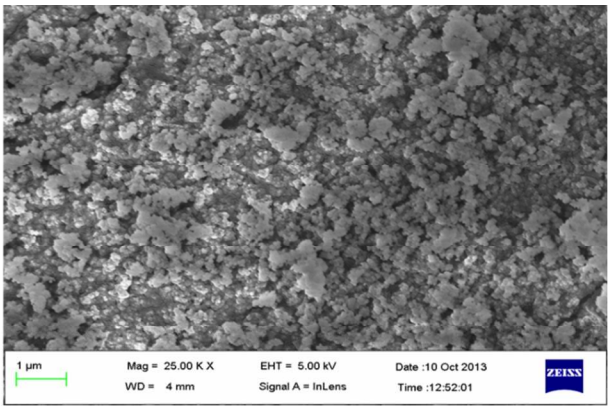

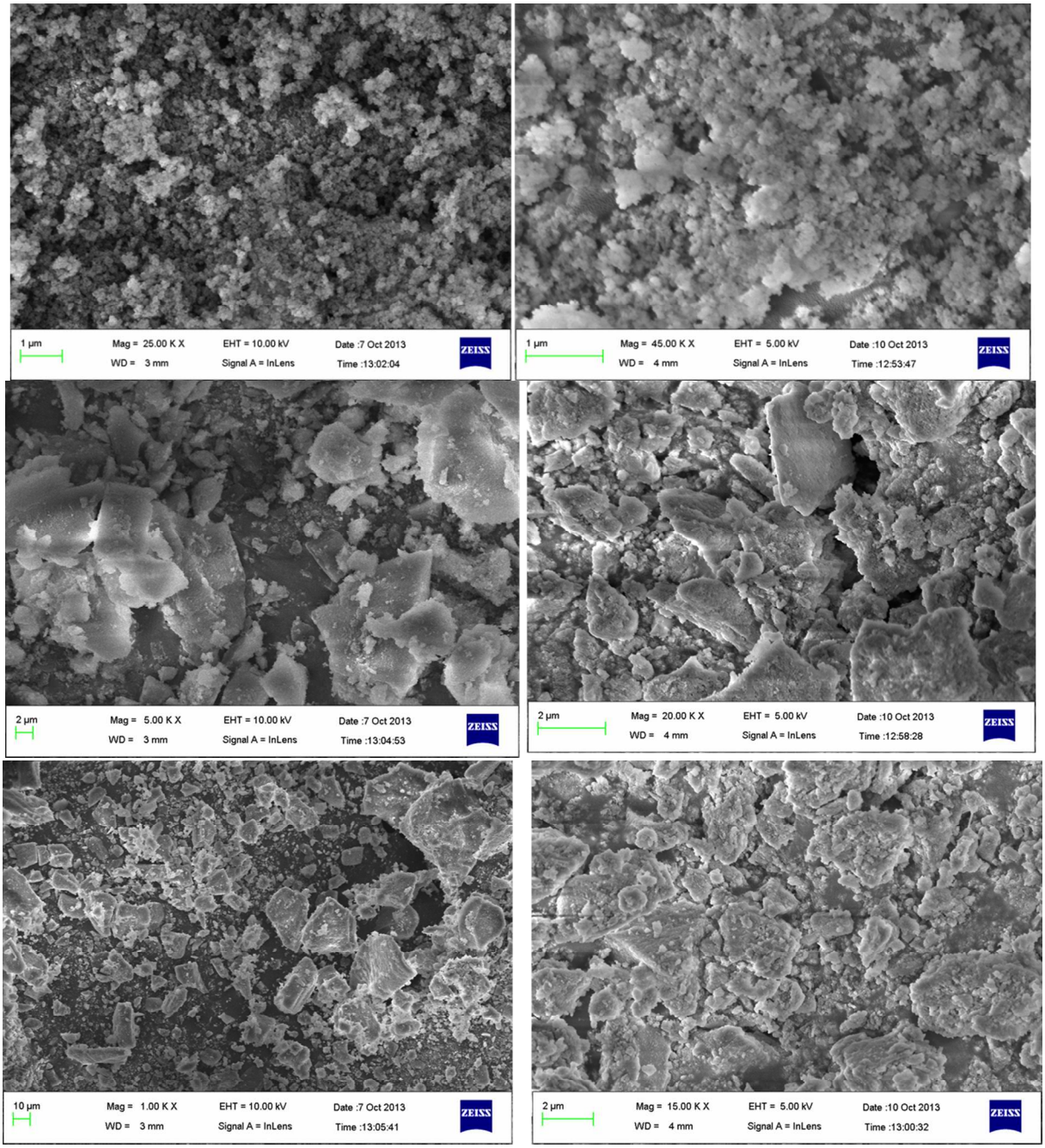

Fig. S1 SEM images of sub-micrometric silica particles doped with different concentrations of alumina. From left to right, particles are at 500 ^{0}C to 900 ^{0}C; top to bottom shows different concentration of alumina in silica particles, by row from the top (silica:alumina): (1:0.1), (1:0.25), (1:0.35), (1:0.5), (1:0.65), and (1:0.75).